Journal **XX** (XXXX) XXXXXX https://doi.org/XXXX/XXXX

Postscript

Final Published Version:

Titolo: Electronic properties of carbon nanotubes as detected by photoemission and inverse photoemission

Autori:Soncini, Cristian; Bondino, Federica; Magnano, Elena; Bhardwaj, Sunil; Kumar, Manvendra; Cepek, Cinzia; Pedio, Maddalena

Nanotechnology Volume 32, 105703

Citation Soncini et al. Nanotechnology 32, 105703 (2021)

DOI:10.1088/1361-6528/abce30

https://dx.doi.org/10.1088/1361-6528/abce30

Journal **XX** (XXXX) XXXXXX https://doi.org/XXXX/XXXX

Electronic properties of Carbon Nanotubes as detected by Photoemission and Inverse Photoemission

Cristian Soncini[1,2*], Federica Bondino[1], Elena Magnano[1,3], Sunil Bhardwaj[1], Manvendra Kumar[4], Cinzia Cepek[1] and Maddalena Pedio[1]

[1] Istituto Officina Materiali (CNR-IOM), Laboratorio TASC, I-34149 Trieste (Italy)
[2] Dipartimento di Fisica, Università di Trieste
[3]Department of Physics, University of Johannesburg, PO Box 524, Auckland Park 2006, South Africa
[4]Department of Physics, Institute of Science, Shri Vaishnav Vidyapeeth Vishwavidyalaya, Indore 453111, India

E-mail: soncini@iom.cnr.it

Received xxxxxx
Accepted for publication xxxxxx
Published xxxxxx

Abstract

The relation between morphology and energy level alignment in carbon nanotubes (CNT) is a crucial information for the optimization of applications in nanoelectronics, optics, mechanics and (bio)chemistry. Here we present a study of the relation between the electronic properties and the morphology of Single Wall CNTs (SWCNT) and aligned and unaligned Multiwall CNTs (MWCNT). The CNT were synthesized via catalytic chemical vapor deposition in ultra-high vacuum conditions. Combined Ultraviolet Photoemission (PES) and Inverse Photoemission (IPES) spectra reveal a high sensitivity to the nanotube morphology. In the case of unaligned SWCNT the distinctive unoccupied Van Hove Singularities (vHs) features are observed in the high resolution IPES spectra. Those features are assigned to semiconducting and metallic SWCNT states, according to calculated vHs DOS. The two MWCNT samples are similar in the diameter of the tube (about 15nm) and present similar filled and empty electronic states, although the measured features in the aligned MWCNT are more defined. Noteworthy, interlayer states are also revealed. Their intensities are directly related to the MWCNT alignment. Focussing and geometrical effects related to the MWCNT alignment are discussed to account the spectral differences.

Keywords: Carbon Nanotubes, Photoemission, Inverse Photoemission, Van Hove Singularities

1. Introduction

Carbon nanotubes (CNT) are the subject of intense scientific research because of their exceptional set of physical properties, including ultrahigh stiffness, excellent carrier mobility, and structural control of their electronic band structure. CNT combine unique nanostructure with excellent mechanical and electronic properties, and have shown promising applications in several fields, as transistors [1,2], photovoltaic devices[3, 4], supercapacitors [5,6].

Several methods were employed to synthesize carbon nanoscale materials, such as arc discharge, chemical vapor deposition (CVD), plasma method and laser ablation [7]. Today, CNT growth by CVD is a highly controlled process.

The desired characteristic of the CNT are determined by the deposition parameters and different catalytic processes can be used: pyrolysis of iron phthalocyanine, decomposition of acetylene, methane and alcohol over metal catalysts films (iron, palladium, alumina-supported palladium, palladium-germanium) [8]. Crucial information for CNT applications is the understanding of the mutual relation between structural and electronic details. X-ray absorption (XAS) and photoemission spectroscopy (PES) are versatile techniques to study the electronic structure and composition and are widely used for the characterization of carbon nanostructured materials [9, 10, 11]. In particular, Valence Band (VB) PES spectra measure the π and σ bands electron density, respectively related to p_z and sp^2 orbitals of CNT [12,13,14,15]. XAS is a powerful tool to accurately study the local density of empty electronic states of a selected element. In carbon-based materials, the C K edge XAS is standardly employed to obtain experimental information on the unoccupied Carbon p-states. On the other hand, Inverse Photoemission (IPES) experiments provide the approximate measure of the total density of the empty states (i.e. the spectra are proportional to the Conduction Band CB). In previous works [16, 17, 18, 19, 20, 21] the sensitivity of IPES was explored for different types of carbon structures (fullerenes, graphite, helicoidal, and straight carbon nanofibers, whisker-like nanotube-nanofibers among others), allowing the detection of the electronic occupied states counterpart, i.e. π^* and σ^* bands. IPES information is similar to XAS, though is not element sensitive and no core hole are formed during the measurements process [22, 23].

The electronic band structure of Single Wall CNT (SWCNT) can be derived by cutting the band dispersion of a graphene sheet along specific parallel lines in the reciprocal space or in other words, applying periodic boundary conditions on a rolled-up graphene lattice with only discrete momenta along the circumference. As a consequence, the density of states (DOS) of SWCNT is also characterized by Van Hove singularities (vHs), which depend on the chirality and diameter of the tube. Nevertheless broadening effect have to be carefully considered when comparing calculated vHs DOS with experimental data. A first broadening effect, generally not considered in theoretical vHs DOS, is the lifetime of the hole state created after the electron photoemission. This effect is present also in chirality-pure SWCNT and strongly dependent on the CNT diameter [24]. Moreover, several groups have reported the observation of vHs from SWCNT samples containing SWCNTs with a range of chirality/diameters [13, 25, 26]. Individual SWCNT samples were studied by scanning tunneling spectroscopy (STS) [9] and well-ordered arrays of SWCNT by PES [12, 13,24, 25, 26] XAS [13, 27, 28] and Electron Energy Loss Spectroscopy (EELS) of the C-K edge [28]. The spectroscopic details of the vHs fine structure with the peculiar electronic properties of SWCNT, are discussed in the literature in terms of functionalization, i.e. charge transfer and rehybridization or chemisorption and physisorption [26, 27].

In the case of Multi Wall CNT (MWCNT) both the filled electronic states, as detected by PES Valence Band (VB) data, and the empty states, as measured by IPES [17-20] and C-K edge XAS spectra in the literature, are characterized by graphitic-like electronic states. Their electronic structure is more complicated than SWCNT due to the presence of an inter-shell morphology. Actually, while SWCNT can be modeled as a rolled graphene sheet, MWCNT is considered as n-layer rolled graphite [29]. Theoretical calculations on MWCNT [30], often focussed on the simplest Double Wall CNT [31,32] show that inter-wall interactions are related to the charge redistribution in the MWCNT, with important consequences in the transport properties. Unfortunately, only a few theoretical studies are present in the literature.

In this work, we compare the combined PES and IPES results of three different CNT samples: mixture of SWCNT, aligned and unaligned MWCNT. The VB spectrum of SWCNT, as expected, shows the vHs typical fingerprint. Moreover, thanks to our IPES high experimental resolution, the vHs in CB at an energy below the π^* state are reported, in agreement with XAS. For the MWCNT samples, combined PES-IPES spectra confirm the main graphitic-like features related to the occupied and empty orbitals. Noteworthy, we found a fine structure of the π^* empty orbital and interlayer states, slightly different for the aligned and unaligned MWCNT.

2. Experiment

2.1 Sample preparation

CNT bundles were synthesized in the INSPECT laboratory of the IOM-CNR, where the catalyst depositions, CVD processes and spectroscopic analysis are all performed in an ultra-high vacuum experimental chambers (base pressure $<1x10^{-10}$mbar). The used substrates were alumina (Al_2O_3) and titanium nitrate (TiN) films grown on silicon wafer. In all the growth procedures Fe films (99.99% pure, deposited *in situ* before CVD by electron beam evaporation, thickness: 4nm) were used as catalysts, while acetylene as the precursor gas. Following the procedures of Ref. 34, to control the strong diffusion of the catalyst into the TiN substrate, we obtained different CNTs yields by performing or not an annealing pre-treatment of the TiN substrate at 600°C before Fe deposition. Fine details of the CVD parameters and XPS characterization of the CNTs grown on Al_2O_3 and TiN films are reported in references 33 and 34, 35, respectively. We named as ALC2 the SWCNT grown on Al_2O_3/Si [33], as a-TiN the aligned and TiN the unaligned MWCNT [34,35]. The PES measurements were performed

on CNT samples grown *in situ*. The X-ray Photoemission (XPS) analysis of the samples is reported in the cited references [33-35].

The IPES and XAS measurements were performed *ex situ*. The samples after introduction in the ultra-high vacuum (UHV) chamber, were heated for a few hours up to about 250 °C to get rid of the surface contaminants, providing PES spectra in agreement with the *in situ* measurements. Further annealing up to about the growth temperature (500°C see refs 32-34) revealed no changes.

2.2 Methods

Normal Incidence IPES spectra were acquired at the CNR-IOM SIPE laboratory. The measurements were performed using a home-made Erdman-Zipf electron gun that provides a highly collimated electron beam. The electron beam divergence was ~2°. Photons emitted by the sample were collected by a home-made Geiger-Müller type detector with He and Iodine gas mixture and a Strontium Fluoride SrF_2 entrance window filtering photons of energy hν=9.5 eV. The experimental resolution was below 0.30 eV, as measured by the Fermi level (E_F) onset of a clean Ta foil. The IPES spectra were normalized at each point to the incident electron beam current. IPES probing depth can be estimated from the mean free path of the typical incident electron energy (Kinetic Energy=4-30 eV) [36, 37] as smaller as 0.7 nm. CNTs were introduced by a load lock. The base pressure was 3 10^{-10} mbar.

The samples were also characterized by Raman Spectroscopy, Scanning Electron Microscopy (SEM), Ultraviolet Photoemission (PES), X-ray Photoemission Spectroscopy (XPS) and C K-edge X-ray Spectroscopy (XAS).

Ultraviolet VB PES spectra of *in situ* samples were acquired in the UHV experimental apparatus (base pressure ~4x10^{-10} mbar) of the INSPECT laboratory, using a conventional He discharge lamp (He II emission: hν = 40.8 eV), and a hemispherical electron energy analyzer (PSP), obtaining an overall energy resolution of ~0.2 eV. All the electron-energy distribution curves were measured at room temperature and in normal emission geometry. The binding energy (BE) of the VB spectra is referred to the Fermi energy level.

Raman Spectroscopy was performed employing a Renishaw Ramascope spectrometer equipped with an Olympus microscope, and a cooled CCD camera as photo-detector. The SEM images were acquired with a ZEISS microscope mod. Supra 40, characterized by an electron energy range of 0.1–30 KeV.

C K-edge Near Edge X-ray Absorption Spectroscopy XAS spectra measurements were carried out at the CNR beamline BACH at the Elettra synchrotron facility in a base pressure < 10^{-9} mbar [38]. XAS spectra were measured in total electron yield (TEY) by collecting the drain current from the sample with a photon energy resolution of ~80 meV. The signal was normalized to the current acquired from a freshly evaporated gold grid placed just before the sample.

3. Results

Figure 1 shows the SEM images of the three samples. The quality and type of CNT were investigated by Raman spectroscopy with laser excitation energy of 514 nm (2.41 eV). The Raman spectra of the ALC2 show relevant differences to TiN and a-TiN samples. In particular, for ALC2 several peaks are revealed in the Radial Breathing Mode (RBM) spectral region. The RBM peak distribution and the low-intensity ratio between the D-Band and G-Band (I_D/I_G) indicate the presence of a mixture of metallic and semiconducting SWCNT with diameters (d), ranging between 0.9 nm < d < 1.9 nm (Table 1). In the a-TiN and TiN samples, no RBM features are detectable. The disorder-induced D-band is strongly enhanced (Fig.SI_1a) and the formation of CNTs with diameters distribution centered at about 15 nm is estimated by SEM (SI_Fig. 2a-b).

The detailed Raman and SEM images analysis of the three samples is discussed in the SI_1 and SI_2 sections respectively.

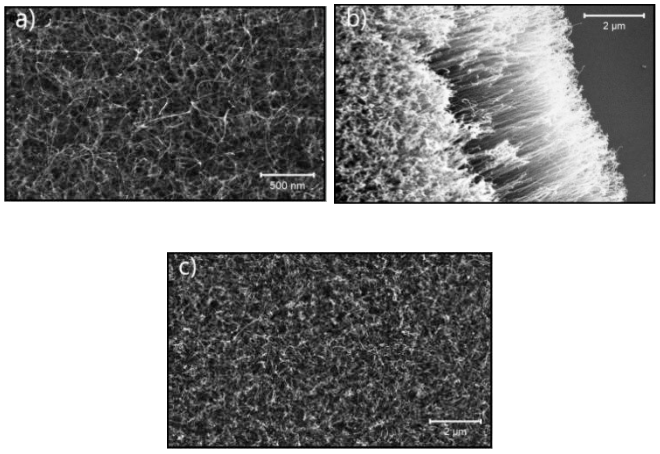

Figure 1 SEM images a) SWCNT ALC2 sample (3 x 1.8 µm^2), b) aligned MWCNT a-TiN (10.5 x 6.5 µm^2) and c) unaligned TiN MWCNT (12.5 x 7.5 µm^2).

3.1 Combined PES-IPES of SWCNT

Figure 2 shows the combined PES-IPES results of the SWCNT ALC2 sample. VB PES and CB IPES data present clear structures due to the π and π * bands respectively (Fig. 2), showing also additional features at lower BE, labeled S1 and M at ±0.45 and about ±1.40 eV.

As discussed in the introduction, the structure and electronic properties of individual SWCNTs can be

determined from the chiral indexes. According to our Raman analysis, the ALC2 sample shows the presence of several RBM frequencies of SWCNT each of them associated with different CNT diameter and chirality (Table 1).

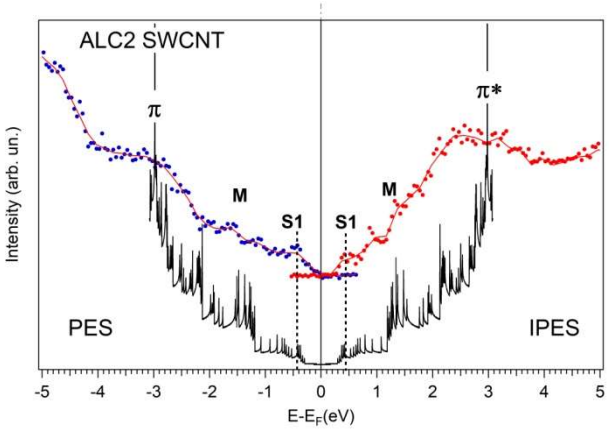

Figure 2 SWCNT ALC2 a) combined PES-IPES spectra and theoretical vHs DOS (solid black line) estimated including all the possible CNT species listed in Table 1. The possible S1 (d~ 1.3 nm) and M (d ~ 0.9 nm) vHs features are labelled, see text for discussion.

RBM frequency (cm^{-1})	**CNT Diameter (nm)**	**Semiconducting SWCNT Chiral Index (n,m)**	**S1 (eV)**
134	1.89	21,5	±0.28
153	1.64	13,11	±0.33
168	1.48	17,3	±0.37
174	1.43	11,10	±0.37
187.5	1.32	12,7	±0.40
205	1.2	12,5	±0.42

RBM frequency (cm-1)	**CNT Diameter (nm)**	**Metallic SWCNT Chiral Index (n,m)**	**M (eV)**
223	1.1	8,8	±1.16
232	1.05	9,6	±1.20
247	0.99	10,4	±1.23
266.5	0.91	12,0	±1.25

Table 1 RBM frequencies, chiralities and related first vH singularity associated with the CNT diameters of the SWCNT ALC2 sample as obtained by Raman analysis (SI_1 section). **top** semiconducting SWCNT, **bottom** metallic SWCNT. The vHs are obtained by the DOS calculated from ref. 24.

Depending on the growth conditions, a mixture of SWCNT with different chirality, diameter and character (metallic or semiconducting) can be formed, each characterized by distinct vHs features. Several PES studies detected vHs in SWCNT samples, see for examples references [13] and [15]. In the case of chirality-pure SWCNT samples VB revealed significant spectral broadening of the VB vHs, not accountable to sample chirality mixture or instrument resolution [24]. This broadening is attributed to the SWCNT intrinsic photo-hole life time, which results directly related to the chirality and diameter of the tube. Moreover, in unpurified SWCNT samples (mixed chiralities, diameters and CNT types) measured by spectroscopies, a significant additional broadening of the signal is revealed when compared to the calculated DOS. Summarizing, mixed SWCNT samples have different superimposed vHs DOS resulting in a diameter dependence of the PES-IPES signal [24].

The calculated vHs DOS in Figure 2 was obtained considering the contribution of each SWCNT listed in the Table 1. The specific SWCNT vHs states are obtained by the DOS calculated from ref. 24 for those tubes found in Raman. As shown in Figure 2 the calculated vHs DOS (black solid line) well correspond to the VB structures, though the presence of further types of SWCNT can not be excluded. Thus, the two peaks S1 and M are not assignable to a unique SWCNT chirality respectively, but are more likely due to a signal overlap of few different SWCNT types present in our sample as discussed in a similar case in ref. 24. The S1 is related mainly to semiconducting SWCNT and M to metallic SWCNTs. The features lying at intermediate energies between S1 and M could tentatively be assigned to S2 peaks overlapping.

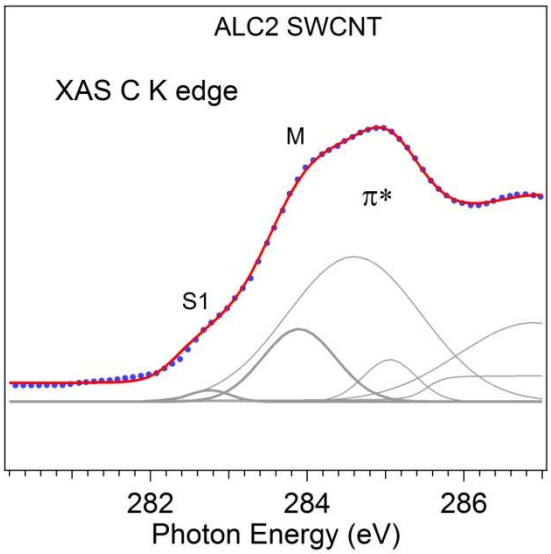

Figure 3 C-K edge XAS taken in TEY mode compared with the results of the fit (red line) and the analysis components (lines).

To verify the π* unoccupied vHs, we measured the XAS C-K edge of ALC2, as shown in Figure 3. The overall shape of C-K edge XAS of SWCNTs, exhibits the well known π* resonance at 285.4 eV and the σ* threshold at 291.7 eV (reported in the SI_4 section). Additionally the π* resonance shows the characteristic fine structure attributed to unoccupied vHs in the electronic density of empty states of SWCNT. In the case of C K edge XAS of SWCNT, fine structure of the π* resonance due to vHs empty states were observed, [13, 27, 28]. Broadening and weak XAS fine structures were observed in some cases [21, 22] depending on the purity of the CNT bundles. The C-K edge XAS data were fitted following the procedure of ref. 13 and 25.

The two additional features at energies below the unoccupied π* band are detected. The components S1 and M (thicker lines) in the XAS (Fig. 3) are compatible with our IPES assignment [39], confirming the assignements of Figure 2.

3.2 Combined PES-IPES MWCNT

Figure 4 shows the combined PES-IPES measurements of the two a-TiN and TiN MWCNT samples.

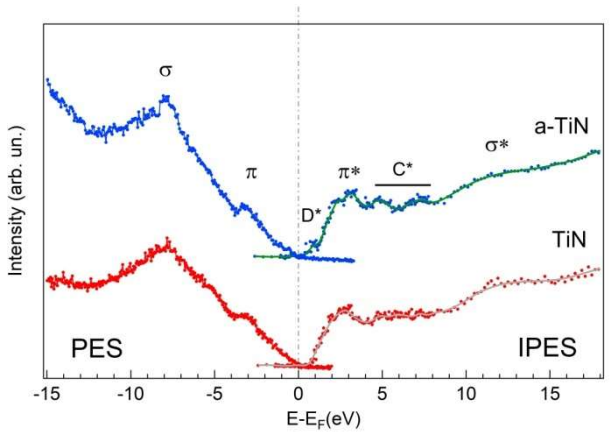

Figure4 Combined PES-IPES results of the aligned a-TiN and no-aligned TiN MWCNT samples.

The mean diameter for both samples is about 15 nm (SI_2 section), but a-TiN results in aligned CNTs, while TiN shows a bundle of CNTs, with no defined orientation. The spectral features are similar in the two samples, though presenting different details. The PES HeII VB spectra in figure 4 exhibits the two characteristic π and σ bands reminiscent states of the graphite band structure, related to the nanotube p_z and sp^2 orbitals, located respectively at about 3 eV and 8 eV [15, 40]. The occupied π features of TiN shows a higher broadening and a lower intensity in comparison to a-TiN. Moreover, in both filled and empty states, the π and π* bands of a-TiN lie at slightly different BE. A similar behaviour was detected by spectro-microscopy PES in ref. 15 and interpreted asa change in band bending of the tube tips in the case aligned CNTs samples.

Concerning the empty electronic states, the MWCNT IPES spectra display two main features, a narrower peak at about 2.5-3.2 eV and a broadband at about 12 eV in substantial agreement with the literature [17-20,41,42]. In the case of large diameter MWCNTs, a reconstruction of their IPES spectrum is modelled by averaging the IPES data of a flat HOPG surface at different incidence angles [42]. Hence the two features are assigned even in unfilled case to the graphitic-like empty π* and σ* bands. The comparison of the MWCNT CB in Figure 4 shows that the π* band of a-TiN is more defined than the π* band of TiN. A splitting of the π* orbitals has been detected in EELS spectra of MWCNT [43] and XAS [44] and ascribed either to the convolution of the vHs or to defects, respectively.

The σ* band results slightly more defined in the case of the unaligned MWCNT.

In the model of IPES spectra for MWCNT described in ref 42, the intensity of the first π* state has been related to an electron focusing effect, which is dependent on the average tube diameter and the impinging electron kinetic energy. Highly collimated electrons approaching the CNT (as in the case of IPES) induce an image charge potential on the tube. This potential bends the trajectories of the electrons, focusing them around the CNT and effectively increasing the cross-sectional area of the tubes, making the spetra sensible mainly to the outmost shells. This effect is dependent on the CNT diameter and the electrons flux energy, resulting stronger for low energy incident electrons (π* more affected rather than σ*).

On the other hand angular resolution can affect the spectra response: in normal incident IPES spectra of the aligned a-TiN sample, most of the incident electrons impinge at the same incidence angle (within the beam angular resolution) with respect to the tube axis increasing the angular contribution in the specific normal direction, whereas the random CNT orientation of TiN bundles leads the incident electrons to couple to states in the whole Brillouin Zone (different electron incidence angles). Either this "geometrical" and the focusing effects could lead to more defined features for aligned CNT.

In the σ* spectral region the focusing effect can be in principle neglected, due to the higher energy of the impinging electron. The I_D/I_G ratio reveals an higher number of defects and amorphous carbon for the a-TiN sample. According to ref. 42, the σ* band is sensible to the CNT quality thus our IPES spectral difference can be accounted to a higher graphitization level of the a-TiN sample in

comparison with the TiN, as verified by Raman measurements (SI_1 section).

In our case in a-TiN, a clear feature is detectable at about 0.9 eV above the Fermi level (feature D* in Fig. 4). In the following, we discuss possible assignments.

The MWCNT theoretical simulation of the electronic structure has not yet been much explored. For the kinetic energies used in IPES measurements, electrons have a short penetration length in a solid, hence the spectra are sensitive to the external out-most shells of the MWCNTs. This implies that we are mainly probing just the few two external shells of the MWCNTs by IPES [42]. A MWCNT consists of graphitic rolled up sheets, each with different diameter, chirality and related vHs. Shell–shell interaction broadens the vHs, and the large number of shells implies that these singularities are quite close to one another, thereby indicating a large number of possibilities of vHs corresponding to different shells. Theoretical and experimental results suggest the presence of discrete states in MWCNT: vHs have been used to illustrate optical properties of MWCNTs [45, 46] and EELS results [43]. Even though vHs have been detected in some cases, in the present samples, presenting a mean outmost shell of about 15 nm, their detection result unlikely (see Supporting Information section 5).

On the other hand, it is worth noting that in the calculated DOS of one and two layers of graphene a shoulder below the π^* resonance is present [47]. In XAS measurements a similar feature is detected for one and two-layer graphene samples, whereas above two layers it is no more detectable, thus attributed to a peculiar unoccupied state of single-layer graphene [43]. We tentatively attribute the D* peak in our IPES spectra to the same origin.

Further angular resolved IPES and PES measurements on aligned nanotubes could enlighten the detected differences between TiN and a-TiN samples more specifically.

In the energy region between the π^* and σ^* bands at about 5-8 eV, a group of features is observed for both samples, labeled C in Figure 4. In the case of HOPG and graphene [48, 49] these features can be related to the peaks of XAS lying in the intermediate energy region between the π^* and σ^* resonances. According to theory, these are states ascribed to interlayer states of the graphite layers, leading to an additional band of three-dimensional character with strong dispersion in the conduction band along the perpendicular direction [48, 49]. Experimentally their existence has been established also in single and few layers of graphene by XAS measurements [47]. In the case of a-TiN these structures are more defined and intense in comparison with the unaligned CNTs. The more defined and intense C structures for a-TiN are assigned to the preferential direction of alignment of the MWCNTs for this sample, whereas the random orientation in TiN leads to a broader and less intense C feature.

4. Conclusions

This work presents the combined PES-IPES results of three different CNT samples providing the electronic structure of these SWCNTs and MWCNTs case systems. The CNTs type and morphology of the three samples were characterized by SEM and Raman spectroscopy resulting in a mixture of metallic and semiconducting SWCNTs for ALC2 and aligned and unaligned MWCNTs for a-TiN and TiN samples. In the case of the SWCNTs, a fine structure is detected at energy below amd above the Fermi level. These filled and empty fine structures were assigned to S1 (semiconducting) and M (metallic) vHs states DOS, as obtained by summing up the different chiralities/diameter DOS present in the CNT bundle.

The MWCNTs samples present spectral differences ascribable to the CNTs different orientation (aligned or not). PES data suggest a slight change of band bending due to tubes alignment, while IPES π^* band is more defined in the case of the aligned CNTs. In the energy region between the π^* and σ^* bands a group of features have been related to interlayer states that are more intense and better resolved in the a.TiN sample.

Supplementary information associated with this article includes Raman analysis, SEM images, C1s XPS results, extended C K edge XAS and high-resolution C1s of the ALC2 sample and vHs energy esteems of large tubes.

Acknowledgments

This work is partially supported by the Italian MIUR through the Progetto EuroFEL (RoadMap Esfri) and the Elettra Proposal number 20180557. The CNR-IOM technical staff members, Stefano Bigaran, Federico Salvador, Paolo Bertoch, Davide Benedetti and Andrea Martin, are kindly acknowledged for their support.

References

[1] Guo X, Liu J, Liu F, She F, Zheng Q, Tang H, Ma M and Yao S, 2017, *Sens. Actuators. B: Chem.* **240**, 1075.
[2] Li X,. Jeong Y J, Jang J, Lim S and Kim S H, 2018, *Phys. Chem. Chem. Phys*. 20, 1210.
[3] Paul S, Rajbongshi B, Bora B, Nair R G and Samdarshi S, 2017 *New Carbon Materials* **32**, 27.
[4] Luo X, Ahn J Y, Y, Park Y S, Kim J M, Lee H W and Kim S H, 2017, *Solar Energy* **150**, 13.
[5] Li L, Lou Z, Han W, Chen D, Jiang K and Shen G, 2017, *Adv. Mat. Technol.* **2**, 1600282.
[6] Li X, Hao C, Tang B, Wang Y, Liu M, Wang Y, Zhu Y, Lu C and Tang Z, 2017, *Nanoscale* **9**, 2178.
[7] Tessonnier J-P, Sheng Su D, 2010, *Chem. Sus. Chem.* **4**, 824–847

[8] Kumar M, Ando Y, 2010, *Journal of Nanoscience and Nanotechnology* **10**, 3739–3758.
[9] Wildoer J W G, Venema L C, Rinzler A G, Smalley R E and Dekker C, 1998, *Nature* **391**, 59;. Odom T W, Huang J L, Kim P and Lieber C M, *Nature* **391**, 62 (1998).
[10] Wang Y-Q, Sherwood P M A, 2004, *Chem. Mater.* **16**, 5427-5436.
[11] Wepasnick K A, Smith B A, Bitter J L, Fairbrother D H, 2010, *Anal Bioanal Chem.* **396**, 1003–1014.
[12] Ishii H, Kataura H, Shiozawa H, Yoshioka H, Otsubo H, Takayama Y, Miyahara T, Suzuki S, Achiba Y, Nakatake M, Narimura T, Higashiguchi M, Shimada K, Namatame H and Taniguchi M, 2003, *Nature* **426**, 540–544.
[13] Ayala P, Miyata Y, De Blauwe K, Shiozawa H, Feng Y, Yanagi K, Kramberger C , Silva S R P, Follath R, Kataura H and Pichler T, 2009, *Phys. Rev. B: Condens. Matter* **80**, 205427.
[14] de los Arcos T, Garnier M G, Oelhafen P, Seo J W, Domingo C, García-Ramos J V and Sánchez-Cortés S, 2005, *Phys Rev B* **71**, 205416.
[15] Suzuki S, Watanabe Y, Kiyokura T, Nath K G, Ogino T, Heun S, Zhu W, Bower C and Zhou O,2001, *Phys. Rev. B* **63**, 245418
[16] Shiozawa H., Ishii H., Kihara H., Sasaki N., Nakamura S., Yoshida T., Takayama Y., Miyahara T., Suzuki S., Achiba Y., Kodama T., Higashiguchi M., Chi X. Y., Nakatake M., Shimada K., Namatame H., Taniguchi M., and Kataura H., 2006, *Phys Rev B* **73**, 075406
[17] Segura R A, Ibáñez W, Soto R, Hevia S and Häberle P, 2006, *J. Nanosci. Nanotech.* **6**, 1945.
[18] Segura R, Tello A and Häberle P, 2007, *Physica Status Solidi (a)* **204**, 1781.
[19] Hevia S A, Ibáñez W, Segura R A and Häberle P 2006, *Brazilian Journal of Physics* **36**, 894-897.
[20] Segura R, Tello A, Cárdenas G and Häberle P, 2007, *Physica Status Solidi (a)* **204**, 513.
[21] Bhardwaj S, Kumar M, Castellarin Cudia C, Pedio M and Cepek C, 2012, *Physica Status Solidi B*, 1–3.
[22] Cook P L, Yang W, Liu X, García-Lastra J M, Rubio A, Himpsel F J, 2011 *J. Chem. Phys*. **134**, 204707.
[23] Mugnaini V, Calzolari A, Ovsyannikov R, Vollmer A, Gonidec M, Alcon I, Veciana J, Pedio M, 2015, *J. Phys. Chem. Lett.,* **6**, 2101−2106.
[24] Shearer C J, Yu L P, Blanch A J, Zheng M, Andersson G G and Shapter J G, 2019, *J. Phys. Chem. C* **123**, 26683−26694.
[25] Rauf H, Pichler T, Knupfer M, Fink J, and Kataura H, 2004, *Phys. Rev. Lett.* **93,** 096805.
[26] Ayala P, Shiozawa H, De Blauwe K, Miyata Y, Follath R, Kataura H and Pichler T, 2010, *J. Mater. Sci.* **45**, 5318–5322.
[27] Kramberger C, Ayala P, Shiozawa H, Simon F, Friedrich A, Liu X, Ruemmeli M, Miyata Y, Kataura H, Hoffmann P, and Pichle1 T, 2011, *Phys Rev B* **83**, 195438.
[28] Castrucci P, Scarselli M, De Crescenzi M, El Khakani M A. Rosei F. *Nanoscale*, 2010, **2**, 1611–1625.
[29] Birò L P, Lambin P 2006 Scanning Tunneling Microscopy of Carbon Nanotubes. In: Popov V.N., Lambin P. (eds) Carbon Nanotubes. NATO Science Series II: Mathematics, Physics and Chemistry, vol 222. Springer, Dordrecht.
[30] Abrikosov A A, Livanov Jr D V and A A Varlamov, 2005, *Phys Rev B* **71**, 165423.
[31] Miyamoto Y, Saito and Tomanek D, 2001, *Phys Rev B* **65**, 041402.
[32] Abdali M and Mirzakuchaki S, 2014, *Mat.Sci. in Semiconductor Processing* **17**, 222–227.
[33] Mattevi C, Wirth C T, Hofmann S, Blume R, Cantoro M, Ducati C, Cepek C, Knop-Gericke A, Milne S, Castellarin-Cudia C, Dolafi S, Goldoni A, Schloegl R Robertson J, 2008, *J. Phys. Chem. C* **112**, 12207–12213.
[34] Esconjauregui S, Bhardwaj S, Yang J, Castellarin-Cudia C, Xie R, D'Arsie L, Makaryan T, Sugime H, Eslava S, Cepek C and Robertson J, 2014, *Carbon* **7**, 3.
[35] Esconjauregui S, Bayer B C, Fouquet M, Wirth C T, Yan F, Xie R, Ducati C, Baehtz C, Castellarin-Cudia C, Bhardwaj S, Cepek C, Hofmann S and Robertson J, 2011, *J. Applied Physics* **109**, 114312.
[36] Wertheim G K, Buchanan D N E, Chaban E E and Rowe J E, 1992, *Solid State Comm.* **83**, 785.
[37] Goldoni A, Cepek C and Modesti S, 1996, *Synthetic Metals* **77**, 189.
[38] Zangrando M, Zacchigna M, Finazzi M, Cocco D, Rochow R and Parmigiani F, 2004, *Rev. Sci. Instrum.* **75**, 31–36
[39] It is worth noting that the sampling depth in IPES is very surface sensitive (at about 1 nm), whereas XAS in TEY probes about than 5 nm, see Kawai J, Adachi H, Hayakawa S, Zheng S, Kobayashi K, Gohshi Y, Maeda K and Kitajima Y, 1994, *Spectrochimica Acta Part B Atomic Spectroscopy* **49**, 739-743.
[40] Choi J, Lee S M, Choi Y C, Lee Y H and Jiang J C, 2001, *Chem. Phys. Letters* **349**, 185-190.
[41] Segura R, Flores M, Hevia S A and Häberle P, 2007, *Microelectronics Journal* **39**, 529.
[42] Hevia S A, Segura R and Haeberle P, 2014, *Carbon* **80**, 50.
[43] Castrucci P., Scilletta C, Del Gobbo S., Scarselli M, Camilli L., Simeoni M, Delley B, Continenza A De Crescenzi M, 2011 Nanotechnology **22,** 115701.
[44] Tang Y H, Zhang P, Kim P S, Sham T K, Hu Y F, Sun X H, Wong N B, Fung M K, Zheng Y F, Lee C S and Lee S T, 2001, *Appl. Phys. Lett.* **79**, 3773.
[45] Brennan M E., Coleman J N, Drury A, Lahr B, Kobayashi T, Blau W J, 2003 Optics Letters, **28**, 266.
[46] Uemura T, Yamaguchi S, Akai-Kasaya M, Saito A, Aono M, Kuwahara Yuji, 2006, Surf. Sci. **600**, L15–L19
[47] Pacile D, Papagno M, Fraile Rodrıguez A, Grioni M, Papagno L, Girit C Ö, Meyer J C, Begtrup G E and Zettl A, 2008, *Phys Rev Lett* **101**, 066806.
[48] Fischer D A, Wentzcovitch R M, Carr R G, 1991, *Phys Rev B* **44**, 1427.

[49] Weser M, Rehder Y, Horn,. Sicot , Fonin M, Preobrajenski, A B, Voloshina E N, Goering E,and Dedkov Yu. S., 2010, *Applied Physics Letters* **96**, 012504.